Research Article

Cancer Prevention Research

Widefield Optical Imaging of Changes in Uptake of Glucose and Tissue Extracellular pH in Head and Neck Cancer

Zhen Luo[1], Melissa N. Loja[2], D. Greg Farwell[3], Quang C. Luu[3], Paul J. Donald[3], Deborah Amott[3], Anh Q. Truong[3], Regina Gandour-Edwards[4], and Nitin Nitin[1,5]

Abstract

The overall objective of this study was to develop an optical imaging approach to simultaneously measure altered cell metabolism and changes in tissue extracellular pH with the progression of cancer using clinically isolated biopsies. In this study, 19 pairs of clinically normal and abnormal biopsies were obtained from consenting patients with head and neck cancer at University of California, Davis Medical Center. Fluorescence intensity of tissue biopsies before and after topical delivery of 2-NBDG (2-[N-(7-nitrobenz-2-oxa-1,3-diazol-4-yl)amino]-2-deoxy-D-glucose) and Alexa 647-pHLIP [pH (low) insertion peptide] was measured noninvasively by widefield imaging, and correlated with pathologic diagnosis. The results of widefield imaging of clinical biopsies demonstrated that 2-NBDG and pHLIP peptide can accurately distinguish the pathologically normal and abnormal biopsies. The results also demonstrated the potential of this approach to detect subepithelial lesions. Topical application of the contrast agents generated a significant increase in fluorescence contrast (3- to 4-fold) in the cancer biopsies as compared with the normal biopsies, irrespective of the patient and location of the biopsy within a head and neck cavity. This unpaired comparison across all the patients with cancer in this study highlights the specificity of the imaging approach. Furthermore, the results of this study indicated that changes in intracellular glucose metabolism and cancer acidosis are initiated in the early stages of cancer, and these changes are correlated with the progression of the disease. In conclusion, this novel optical molecular imaging approach to measure multiple biomarkers in cancer has a significant potential to be a useful tool for improving early detection and prognostic evaluation of oral neoplasia. *Cancer Prev Res; 7(10); 1035–44. ©2014 AACR.*

Introduction

Head and neck cancers continue to be the sixth most common cancer worldwide with approximately 270,000 new oral cavity tumors per year (1). Invasive procedures such as tissue and lymph node biopsies are the standard approaches used for clinical diagnosis and staging of the head and neck cancers (2, 3). There is a need to develop noninvasive molecular imaging approaches to aid in early detection, prognostic assessment, and subsequent longitudinal surveillance after treatment of the disease. Success in clinical translation of these imaging approaches will also enable molecular classification of the disease that may further improve detection sensitivity and/or prognostic assessment of the disease.

To develop a comprehensive molecular imaging approach to aid in detection and prognostic evaluation of head and neck cancers, this study evaluates simultaneous changes in metabolic activity of cells and acidosis in the extracellular domain using clinically isolated tissues. Upregulation of glucose metabolic pathways and a shift from aerobic metabolism to anaerobic metabolism (glycolysis) are the central hallmarks of various cancers, including breast, prostate, colon, head, and neck, and are sensitive indicators of progression of cancer (4, 5). The shift to glycolysis for energy production causes high rates of glucose consumption and also leads to a significant increase in production and release of acidic metabolites (such as protons and lactic acid) in the extracellular matrix (6, 7). Combined with the reduced capability of tumor-associated vasculature to deliver blood-based pH buffer, advanced cancers have an acidic extracellular pH as compared with normal tissue (8). Thus, the reduction of extracellular pH is a key hallmark of cancer progression and is closely associated with increased mutagenesis, metastasis, and resistance to radiation and drug therapies (9–16). Thus, measurement of simultaneous changes in metabolic activity and extracellular pH will have a significant impact on detection and prognosis of cancer

[1]Department of Biological and Agricultural Engineering, University of California, Davis, Davis, California. [2]Department of Surgery, Division of Vascular Surgery, University of California, Davis, Davis, California. [3]Department of Otolaryngology, University of California, Davis, Davis, California. [4]Department of Pathology and Laboratory Medicine, University of California, Davis, Davis, California. [5]Department of Food Science and Technology, University of California, Davis, Davis, California.

Note: Supplementary data for this article are available at Cancer Prevention Research Online (http://cancerprevres.aacrjournals.org/).

Corresponding Author: N. Nitin, UC Davis, One Shields Avenue, Davis, CA 95616. Phone: 530-572-6208; Fax: 530-752-2640; E-mail: nnitin@ucdavis.edu

doi: 10.1158/1940-6207.CAPR-14-0097

and improve understanding of the correlation between changes in metabolic activity and acidosis in clinically isolated cancer biopsies.

Clinically, changes in glucose metabolic activity are measured by PET using a radioactive glucose analog [18F]-fluoro-2-deoxyglucose. Currently, no clinical imaging approach is available for noninvasive measurement of changes in tissue pH with neoplasia. For imaging extracellular acidic environment in tumors, an experimental study using animal model system has investigated a pH-sensitive peptide-based PET imaging agent (17). This pH-sensitive peptide inserts across the lipid bilayer at an acidic extracellular environment (pH < 7.0) but not at a normal physiologic pH. In our recent study, we have demonstrated that topical application of fluorescently labeled pHLIP peptide can detect differences in extracellular pH in clinically abnormal and normal biopsies (18). Furthermore, currently there are no clinical imaging approaches for simultaneous measurement of molecular changes in metabolic activity and extracellular pH with the progression of cancer. Simultaneous measurements of multiple biomarkers in a clinical environment have a potential to improve detection specificity of oral neoplasia as demonstrated by a recent study (19).

Widefield fluorescence imaging was selected as the imaging modality in this study. On the basis of recent developments in optical instrumentation (20, 21), widefield optical imaging is emerging as a clinical approach to aid in detection of localized cancer lesions in patients with head and neck cancer (19, 22). Furthermore, the widefield optical molecular *in vivo* imaging approaches are complementary to the whole-body PET imaging. Similarly, widefield molecular imaging of *ex vivo* biopsy sample is complementary to the standard histology and IHC analysis of tissue sections by providing a rapid assessment of the isolated tissue without the need for sectioning and fixation (23).

In summary, the overall goal of this study was to develop optical molecular imaging approaches to simultaneously measure changes in multiple molecular biomarkers in clinically isolated head and neck biopsies. Evaluation using clinically isolated tissue samples is important as these clinical samples represent heterogeneity of disease among the population. Multiple imaging contrast probes [fluorescent glucose analog 2-NBDG (2-[N-(7-nitrobenz-2-oxa-1,3-diazol-4-yl)amino]-2-deoxy-D-glucose) and Alexa 647–labeled low pH insertion peptide pHLIP] were topically delivered to clinically isolated biopsy specimens, and the resulting contrast in clinically isolated tissues was measured using widefield fluorescence imaging.

Materials and Methods

Probe selection and conjugation

Fluorescently labeled deoxyglucose (2-NBDG) was obtained from Invitrogen. For fluorescent labeling of the pHLIP peptide (ACEQNPIYWARYADWLFTTPLLLLDLALLVDADEGTG), Alexa Fluor 647 C2 maleimide (Invitrogen) was reacted with the thiol (SH-group) of cysteine at the N-terminus of pHLIP to form a stable thioether bond. The details of the conjugation and purification process are described in our prior publication (18).

Collection of paired biopsies

Pairs of clinically normal and abnormal biopsies (2–6 mm in diameter) were obtained from patients who have signed informed consent and are undergoing surgical resection of suspected cancer at the University of California, Davis Medical Center (UCDMC). The paired biopsy samples were kept fresh in cold normal saline (0.9% NaCl), and were transported to the laboratory in less than 30 minutes.

Widefield fluorescence imaging of tissue autofluorescence

To compare the increase in fluorescence intensity of topically labeled tissue samples, widefield fluorescent images before and after staining for each pair of biopsies were acquired. Precontrast images provide a measure of tissue autofluorescence background signal, whereas the postcontrast images measure contributions from both autofluorescence and fluorescence of contrast media labeling. To assess autofluorescence before the application of fluorescent contrast media, the tissue was imaged using a commercially available widefield imaging system (Maestro 2, Cri) at the Center for Molecular and Genomic Imaging, University of California, Davis). For measuring autofluorescence of tissue biopsies in the 2-NBDG channel, the tissues were excited using a 500-nm wavelength light, and the fluorescence emission was collected using a 530- to 600-nm emission filter. For measuring autofluorescence of the tissue biopsies in the Alexa 647-pHLIP channel, the tissues were excited using a 640-nm wavelength light, and the fluorescence emission was collected using a 670- to 800-nm emission filter. The integration time for the camera was maintained constant throughout the study at 100 ms.

Topical labeling of intact biopsies

After autofluorescence imaging, both normal and abnormal paired biopsies were then topically labeled with 2-NBDG and Alexa 647-pHLIP simultaneously. The details of the topical labeling procedure and validation of delivery in biopsy tissues were described in our previously published research article (18). Probe delivery was achieved by topical labeling of isolated biopsy samples with 0.05 mg/mL 2-NBDG and 5 μmol/L Alexa 647-pHLIP in nonbuffered saline with 10% DMSO. After 60 minutes at 37°C, the biopsies were washed in normal saline for 10 minutes to remove any unbound 2-NBDG and Alexa 647-pHLIP.

Postcontrast widefield fluorescence imaging

After removing unbound contrast agents (2-NBDG and Alexa 647-pHLIP) by washing tissue samples in normal saline, the tissue samples were again imaged by widefield imaging system using the same filter configurations for 2-NBDG and pHLIP-Alexa 647 as described in the previous section. Both the pre- and postcontrast images were acquired using the same integration time.

Table 1. Clinically isolated paired biopsies and their pathologic diagnosis

Patient	Clinically "abnormal" location	Pathologic diagnosis	Clinically "normal" location	Pathologic diagnosis
1	Tonsil	Invasive SCC ($n = 9$)	Tonsil	Normal
2A and B	Tonsil		Tonsil	
3A and B	Tonsil		Tonsil	
4	Tonsil		Base of tongue	
5	Epiglottis		Posterior pharynx	
6	Subglottis		Epiglottis	
7	Hard palate		Buccal	
8A and B	Base of tongue	Cis ($n = 2$)	Base of tongue	
9A and B	Base of tongue	Normal ($n = 3$)	Base of tongue	
10	Base of tongue		Buccal	
11A and B	Base of tongue	Normal with chronic inflammation ($n = 2$)	Base of tongue	
12	Tonsil	Moderate dysplasia	Soft palate	
13	Base of tongue	Mild dysplasia	Buccal	
14	Left vallecula	Invasive SCC	Right base of tongue	1/3 normal 2/3 SCC

Abbreviations: Cis, Carcinoma *in situ*; SCC, squamous cell carcinoma.

Quantification of imaging data

For quantification of widefield images collected using the Maestro 2 Imaging system (CRi), both the white light and fluorescence images of biopsy samples were analyzed using ImageJ (Public domain, NIH). The whole-tissue area was firstly selected in white light image by drawing the region of interest around the edge of the tissue (illustrated in Supplementary Fig. S3). The selected region identified in the white light image was overlaid on the corresponding fluorescence image. The mean fluorescence intensity (MFI) of the selected region was then calculated using ImageJ. To compare the MFI between cancer and normal biopsy samples across all patients, the average MFI was calculated by averaging the MFI from all isolated biopsies from individual patients.

The changes in MFI before and after topical delivery of contrast agents in each biopsy samples were calculated as follows: $\Delta MFI = MFI_{Postcontrast} - MFI_{Precontrast}$.

To compare the difference in ΔMFI between unpaired samples, the average ΔMFI of all cancer biopsy samples and average ΔMFI of all unpaired normal samples were calculated.

The differential contrast ratio based on the ΔMFI of the clinically abnormal biopsy and the paired clinically normal biopsy was calculated as follows: $Ratio = \Delta MFI_{Abnormal}/\Delta MFI_{Normal}$, where $\Delta MFI_{Abnormal}$ is the ΔMFI of the clinically abnormal biopsy sample and ΔMFI_{Normal} is the ΔMFI of the paired clinically normal biopsy sample.

The quantified imaging results from fluorescence imaging were analyzed using Microsoft Excel 2007 (Microsoft Inc.) and SAS (version 9.1 SAS Inc.). The Student *t* test was used for evaluating statistical significance between the treatments.

Pathologic diagnosis

The tissue biopsies were fixed after the postcontrast imaging of the tissues. The fixed tissues were submitted to the pathology department for slicing and hematoxylin and eosin (H&E) staining. The prepared slides were evaluated by a board-certified pathologist at the University of California, Davis (Regina Gandour-Edwards). The results from fluorescence imaging measurements were correlated with the pathologic diagnosis.

Results

Clinically isolated biopsies

Table 1 shows the diverse anatomical locations within the head and neck cavity from which the paired biopsies were isolated and their corresponding pathologic diagnosis. Fourteen consenting patients at UCDMC provided 14 clinically normal biopsies and 19 distinct clinically abnormal biopsies. Patients ranged from 51 and 84 years old, and 75% were male. All of the patients were white and had no prior history of oropharyngeal carcinoma. When multiple abnormal biopsies were obtained, they were collected from the same anatomical region but distinct locations within the tumor. The clinically isolated biopsies after evaluation with the selected molecular contrast probes were fixed, stained, and evaluated by a board-certified pathologist.

Widefield imaging of topically applied 2-NBDG and pHLIP in paired clinically normal and abnormal biopsies

The results in this section demonstrate simultaneous imaging of changes in glucose metabolic activity and extracellular pH in clinically isolated paired biopsies (Fig. 1). Precontrast images were acquired before topical delivery of

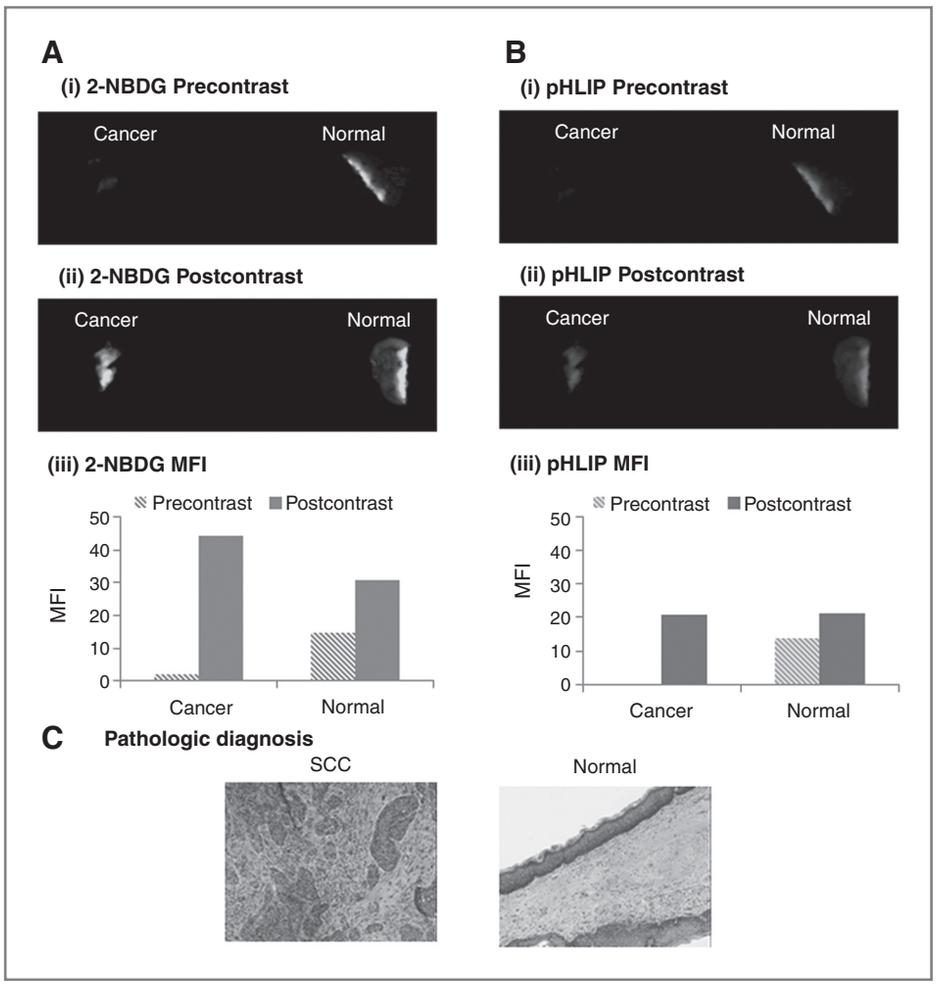

Figure 1. Illustration of simultaneous imaging of changes in glucose metabolic activity and extracellular pH in clinically isolated paired biopsy specimens. Representative widefield fluorescence images of a paired biopsy set before (precontrast) and after (postcontrast) topical application of 2-NBDG [A(i) and A (ii)] and Alexa 647-pHLIP [B(i) and B(ii), respectively. MFI of the corresponding pre- and post widefield imaging measurements using 2-NBDG [A(iii)] and Alexa 647-pHLIP [B(iii)], respectively. C, corresponding pathologic H&E images of the paired cancer and normal biopsies.

2-NBDG to assess the autofluorescence signal intensity of each biopsy sample. Figure 1A(i) shows the results from a paired biopsy sample in which the clinically abnormal sample has a significantly lower autofluorescence signal intensity as compared with the corresponding clinically normal biopsy specimen. In the postcontrast images (after topical delivery of 2-NBDG; Fig. 1A(ii)), the fluorescence signal from the clinically abnormal biopsy shows a significant increase in fluorescence contrast as compared with the paired clinically normal biopsy.

The MFI was calculated for both the clinically abnormal and normal biopsies before and after topical application of 2-NBDG (Fig. 1A(iii)). The MFI before staining represents the contribution from tissue autofluorescence, and the MFI after staining represents the contribution from both tissue autofluorescence and 2-NBDG uptake. Results demonstrate a substantial increase in fluorescence intensity of the clinically abnormal biopsy sample as compared with the clinically normal biopsy. On the basis of the pathology evaluation, the clinically abnormal biopsy was diagnosed as squamous cell carcinoma and the clinically normal biopsy was diagnosed as normal. Histologic images of these clinically abnormal and normal biopsy are shown in Fig. 1C.

Figure 1B(i and ii) shows the representative widefield fluorescence images of the biopsy samples imaged using the emission wavelength range of 670 to 800 nm. This wavelength range was used for imaging tissue contrast generated upon binding of Alexa 647–labeled pHLIP peptide. Similar to the approach outlined for the 2-NBDG, the tissue biopsies were imaged before application of contrast agent to determine the background autofluorescence of the tissue in the wavelength range of 670 to 800 nm (Fig. 1B (i)). After topical delivery of pHLIP in tissue samples, substantial increase in fluorescence intensity was noticed in the clinically abnormal biopsy, whereas there was a small increase in fluorescence intensity of the clinically normal tissue (Fig. 1B(ii)).

Figure 1B(iii) shows the MFI for both the pre- and postcontrast widefield fluorescence images of clinically abnormal and normal biopsies. The quantified imaging results illustrate that the MFI increased significantly in the clinically abnormal biopsy as compared with the paired normal biopsy isolated from the same patient. Overall, the trend observed with 2-NBDG and pHLIP-based contrast agents shows selective and significant increase in fluorescence contrast in a clinically abnormal biopsy (pathologic

diagnosis: squamous cell carcinoma) as compared with the pathologically and clinically normal biopsy.

Differences in fluorescence contrast between clinically abnormal and normal biopsies were independent of the tissue autofluorescence levels

Changes in tissue autofluorescence induced by neoplasia have been used as an optical biomarker for detecting head and neck cancer (24–26). In many of the paired biopsy sets, the autofluorescence signal intensity of the normal biopsy was higher than the paired abnormal biopsy. In contrast to this trend, the autofluorescence signal intensity of the certain clinically normal biopsies was lower than the paired clinically abnormal samples ($n = 5$ in the 2-NBDG fluorescence channel and $n = 3$ in the Alexa 647 fluorescence channel). Figures 2A(i) and B (i) illustrate an example of a clinical case in which the autofluorescence signal intensity of the clinically and pathologically normal sample (precontrast) was lower than the autofluorescence intensity of the clinically and pathologically abnormal sample. However, another clinically abnormal biopsy sample taken from the same patient and from the same anatomical area shows lower autofluorescence intensity than the paired normal tissue (Fig. 2, cancer 2). This dataset indicates that the differences in autofluorescence can also be due to a variety of pathophysiologic factors including neoplasia (25, 27).

Figures 2A(ii) and B(ii) show the postcontrast images of the paired biopsy sets from a patient (two clinically abnormal biopsies and one clinically normal biopsy). After topical delivery of 2-NBDG and pHLIP in the tissue samples, a substantial increase in fluorescence intensity was noticed in both the clinically abnormal biopsies, whereas there was a small increase in fluorescence intensity of the clinically normal tissue. The quantification of the MFI is shown in Figs. 2A(iii) and B(iii). The corresponding histology and pathologic diagnosis for these biopsy samples is shown in Fig. 2C(iii). The results show that both the clinical abnormal biopsies were diagnosed as squamous cell carcinoma, and the clinically normal biopsy was diagnosed as pathologically normal. These results demonstrate that enhancement in fluorescence contrast resulting from specific uptake of 2-NBDG or binding of the pHLIP peptide in diseased biopsy specimens is not significantly influenced by the native autofluorescence properties.

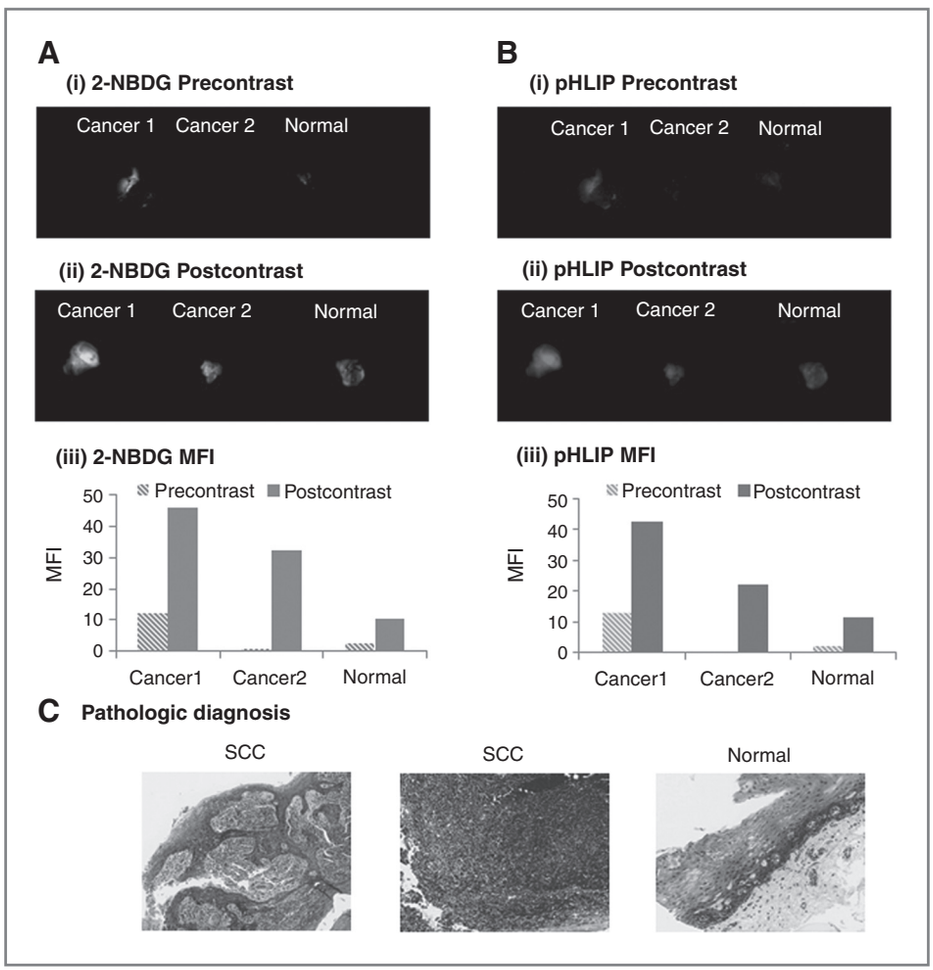

Figure 2. Changes in contrast properties of clinically abnormal and normal biopsies following topical application of contrast agents were independent of the tissue autofluorescence levels. Representative widefield fluorescence images (pre- and postcontrast) of a paired biopsy set in which one of the clinically abnormal biopsies (Cancer 1) had a higher level of autofluorescence in both 2-NBDG [A(i) and A(ii)] and Alexa 647-pHLIP [B(i) and B(ii)] channels as compared with the paired normal biopsy. MFI of the corresponding pre- and post widefield imaging measurements using 2-NBDG [A(iii)] and Alexa 647-pHLIP [B(iii)], respectively. C, corresponding pathologic H&E images of the biopsy set (paired clinically abnormal and normal biopsies).

Sensitivity of 2-NBDG and pHLIP in detecting subsurface lesions

Results in Fig. 3 illustrate an example of a clinical case in which the clinically normal biopsy had invasive cancer underlying the normal epithelial tissue. The precontrast images of the paired biopsy set illustrate that the clinically normal biopsy has a lower autofluorescence signal in both the 2-NBDG and the Alexa 647-pHLIP emission channels as compared with clinically abnormal biopsy. After simultaneous topical labeling of the biopsies with 2-NBDG and Alexa 647-pHLIP, the postcontrast images illustrate a significant increase in fluorescence contrast in both the clinically normal and abnormal biopsies as shown in Figs. 3A (ii) and B(ii). On the basis of the quantification of the MFI for pre- and postcontrast images, the results in Fig. 3A (iii) show that after staining with 2-NBDG, the MFI of the normal biopsy was similar to the MFI of the paired clinically abnormal biopsy. This is particularly significant because the MFI of the normal biopsy was lower than the paired abnormal biopsy in the precontrast images. Quantification of the MFI for the Alexa 647-pHLIP–labeled biopsies in Fig. 3B(iii) also shows a significant increase in the MFI of both the paired clinically abnormal and normal biopsies in the postcontrast images.

Results of pathologic analysis revealed that the clinically normal biopsy had an invasive cancer underneath the normal epithelial section (Fig. 3C(iii)). The histologic analysis indicated that the invasive cancer covered over 2/3 width of the biopsy sample underlying a normal epithelium. In this case, the normal appearance of the tissue influenced the clinical impression of the tissue and without the biopsy it was not possible to clinically detect the presence of invasive disease.

Using a combination of topically applied contrast agents (both 2-NBDG and Alexa 647-pHLIP) and widefield fluorescence imaging, the optical imaging approach was able to detect disease underlying a normal epithelium. This result reflects that the combination of topically applied contrast agents and widefield imaging cannot only detect surface lesions but also aid in detection of subsurface lesions that are often difficult to detect based on visual impression of the tissue.

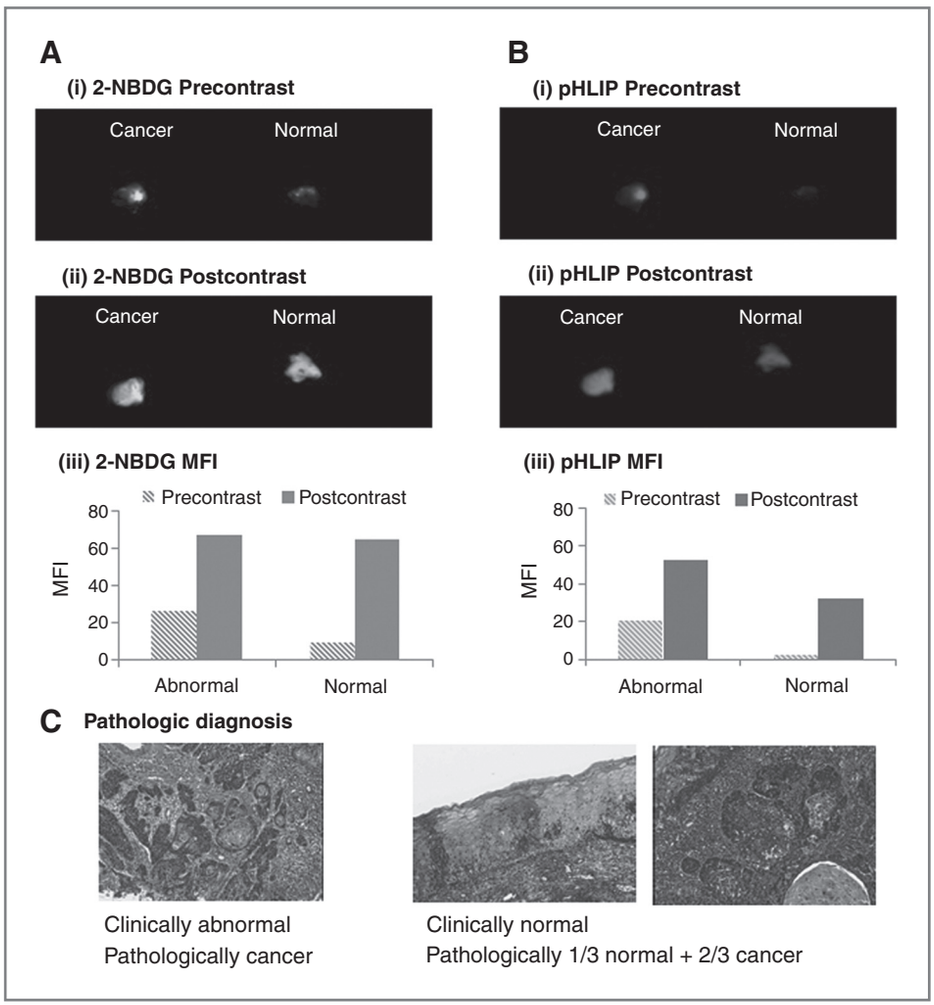

Figure 3. Sensitivity of 2-NBDG and Alexa 647-pHLIP to detect subsurface lesions. Widefield fluorescence images of a pair of biopsies before (precontrast) and after (postcontrast) topical application of 2-NBDG [A(i) and A (ii)] and Alexa 647-pHLIP [B(i) and B (ii)], respectively. MFI of corresponding pre- and post widefield imaging measurements using 2-NBDG [A(iii)] and Alexa 647-pHLIP [B(iii)], respectively. C, corresponding pathologic H&E images of the paired clinically normal and abnormal biopsies. In this case, the clinically normal biopsy had an invasive cancer (over 2/3 width) underneath the normal epithelial section.

2-NBDG uptake and pHLIP binding across all cancerous biopsies

Figure 4A compares the average ΔMFI in cancer biopsies (i.e., the average increase of MFI between post- and precontrast images) with the normal biopsies across all patients with cancer in this study irrespective of the anatomic location within the head and neck cavity. This analysis compares the increase in the mean fluorescence contrast based on uptake of 2-NBDG and binding of pHLIP peptide across all cancer and normal biopsies (i.e., the tissue samples are unpaired). Results showed the average ΔMFI of cancer biopsies ($n = 11$) was significantly higher (approximately 2.5- and 3.3-fold) as compared with the average ΔMFI of normal biopsies ($n = 7$; $P = 0.003$) after topical delivery of 2-NBDG and pHLIP, respectively. These results demonstrate the potential of using fluorescence-labeled glucose and pHLIP to distinguish clinically abnormal tissues from normal tissues across diverse patients by comparing the ΔMFI. The results of average MFI of all biopsy samples before (precontrast) and after (postcontrast) topical delivery with 2-NBDG and pHLIP are shown in the Supplementary Fig. S1.

Correlation between changes in 2-NBDG uptake and pHLIP binding with stages of neoplasia

To compare the changes in metabolic activity and extracellular activity with development of neoplasia, the average differential contrast ratio was calculated between the ΔMFI of pathologically abnormal biopsies with respect to the ΔMFI of paired normal biopsies. This average contrast ratio was calculated separately for the 2-NBDG and the Alexa 647-pHLIP and was plotted as a function of pathologic diagnosis in Fig. 4B.

The results show a multifold increase in the differential contrast ratio between the paired diseased and normal biopsies and the average contrast ratio increased with an increase in severity of the disease. The average contrast ratio for the cancer biopsies ($n = 9$) was approximately 3- and 5.9-fold higher as compared with the pathologic normal biopsies stained with 2-NBDG and Alexa 647-pHLIP, respectively. For the carcinoma *in situ* cases ($n = 2$), the increase in ratiometric contrast was approximately 1.8- and 3.3-fold as compared with normal biopsies stained with 2-NBDG and Alexa 647-pHLIP, respectively. For the dysplasia cases ($n = 2$), the increase in ratiometric contrast was approximately 1.21- and 1.7-fold as compared with normal biopsies stained with 2-NBDG and Alexa 647-pHLIP, respectively. Overall, these results indicate that significant changes in both metabolic activity and extracellular pH can be detected in clinically abnormal biopsies as compared with the paired normal biopsies. The results also show the pHLIP labeling does result in a relatively higher ratiometric contrast ratio in paired biopsy sets as compared with 2-NBDG at all stages of the disease.

In Fig. 4B, the results also show the cases in which clinically abnormal biopsy was diagnosed as normal biopsy based on pathology evaluation. For the pathologically normal biopsies, despite appearing abnormal clinically, the

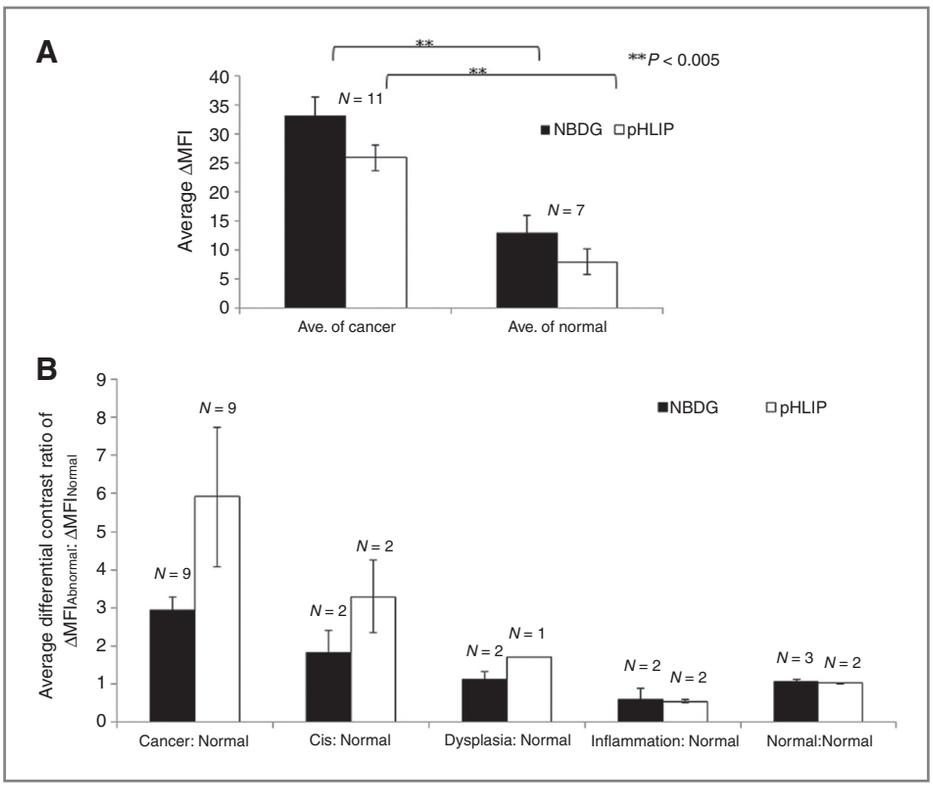

Figure 4. A, average ΔMFI across all cancer and normal biopsy samples before and after topical delivery of 2-NBDG and pHLIP. B, the comparison of average differential contrast ratios of paired biopsy samples as a function of pathologic diagnosis after staining with 2-NBDG and pHLIP, respectively.

ΔMFI of 2-NBDG uptake ($n = 3$) and pHLIP binding ($n = 2$) was similar to the ΔMFI of paired normal biopsies. These biopsies were further confirmed as normal based on the pathology review. These results demonstrate specificity of 2-NBDG and pHLIP-based imaging approaches to distinguish true pathologically cancer biopsy from normal biopsies.

Discussion

Topical delivery of contrast agents enables molecular analysis of intact tissues

Topical delivery is a noninvasive approach to deliver molecular contrast agents to localized tissues. A topical delivery approach provides rapid access to the epithelial tissue and overcomes significant limitations of the alternative delivery approaches, such as intravenous delivery of contrast media. These limitations include nonspecific retention of contrast agents in organs, such as liver and kidney, and delay in imaging time to allow for clearance of the contrast media from the circulation. The results of this study demonstrate that topical delivery of contrast agents to *ex vivo* biopsies was an efficient approach for the delivery of both small molecular weight contrast agent [2-NBDG, molecular weight (MW): 342 Da) and a short peptide (pHLIP, MW: 3,000 Da). These results are in agreement with the results of our prior studies (28, 29). Results in Fig. 3 also demonstrate that the molecular contrast agents were able to target the subepithelial lesions using topical application. This result is also in agreement with the results presented in our recent study (18).

To translate topical delivery of contrast agents to *in vivo* application in a clinical setting, further research is needed to develop topical oral formulations. It is desired that these topical formulations have mucoadhesive properties and provide rapid delivery of imaging contrast agents to target tissues. The mucoadhesive properties will enable localized application of the contrast agents at target sites within the head and neck cavity. In the current literature, various mucoadhesive formulations have been developed for the delivery of therapeutic molecules (30–32). The applications of these therapeutic molecules range from suppressing inflammation (32), prevention of cancer (30, 31), and treatment of localized infections (33) in the oral cavity. These topical delivery approaches provide a framework to adapt these concepts for the delivery of imaging contrast agents. To achieve rapid and uniform delivery of imaging agents, the existing topical formulations can be further modified to include triggered release mechanisms or rapidly eroding polymer formulations (34).

Specificity of 2-NBDG and pHLIP in detection of precancerous and cancerous lesions

The results of this study demonstrate high specificity of both 2-NBDG and pHLIP in detection of both precancerous and cancerous lesions. The specificity is highlighted by the facts that both the molecular contrast agents accurately distinguished the pathologically normal and abnormal biopsies. In this study, three biopsy samples that were considered as clinically abnormal based on the physical examination were found to be normal based on pathologic diagnosis. In the evaluation of these paired biopsies using molecular contrast agents, the clinically abnormal-appearing tissue (but pathologically normal) biopsies did not show a significant increase in fluorescence contrast as compared with the paired clinically and pathologically normal tissues. For further clinical translation, specificity of this approach for discriminating other clinical symptoms such as infections may be further evaluated.

Evaluation of paired biopsies using molecular contrast agents improved the specificity of detecting cancerous lesions as compared with their evaluation using precontrast imaging measurements only (autofluorescence properties). Results show that the ratio of autofluorescence intensity of cancer biopsies with respect to the paired normal biopsy varied among patients, and significant number of paired biopsy sets had autofluorescence ratio greater than 1 in both 2-NBDG and Alexa-647 channels. It is important to note that the primary focus of precontrast imaging measurements was to normalize variation in endogenous contrast among different tissue biopsies. Thus, the selected wavelengths for precontrast imaging may not be optimal (35) for detecting neoplasia based on autofluorescence properties of the tissues.

In this study, one of the clinically normal biopsy was also diagnosed as a cancer biopsy based on pathology evaluation. Pathologic evaluation showed that the cancer was localized in the subepithelial tissue, whereas the epithelial section of the tissue had a normal anatomical structure. A significant change in fluorescence contrast properties was also observed upon topical application of contrast media in this clinically normal, but pathologically abnormal tissue. These results are significant as the imaging approaches may provide a unique method to differentiate cancer tissue with normal epithelium (subepithelial cancers) which cannot be easily identified clinically.

The specificity of both the molecular contrast agents is also illustrated in the results of Fig. 4A. This result compares the dataset of cancer biopsies across all patients without any pairing of the biopsy specimens. The result shows that even without pairing, the cancer biopsies showed a significantly higher (3- to 4-fold) increase in fluorescence contrast as compared with the normal biopsies. This trend is significant as this comparison is across diverse sites within the head and neck cavity and across diverse patients.

The results of this study also illustrate the potential of the selected molecular imaging probes to detect changes in the precancerous stages (both dysplasia and carcinoma *in situ*) of head and neck cancer. Because the study was conducted at a tertiary care center, the number of biopsies at early stage of the disease is small as compared with the cancer biopsies. To further validate the sensitivity of the selected molecular contrast media to detect early-stage biopsy samples, more biopsy samples from early-stage patients are needed.

Correlation between metabolic activity and acidosis

The results of this study illustrate that upregulation in metabolic activity with development of neoplasia is

correlated with acidosis in extracellular matrix of the tissue. This correlation was observed in both precancerous and cancerous lesions. Changes in both metabolic activity and extracellular pH in precancerous lesions indicate that these molecular transformations are not only a result of changes in tissue vasculature in tumors but are present in early stages (avascular stage) of the disease. This evidence indicates that changes in gene expression associated with upregulated metabolic activity and acidosis, such as activation of hypoxia pathway, are triggered in early stages of the disease, and these changes are significantly enhanced by the time disease becomes invasive. This evidence supports the discussion on the role of acidosis, hypoxia, and glycolysis in progression of disease from dysplasia and carcinoma *in situ* to invasive disease (36). This evidence is also supported by other studies that have indicated the role of acidosis in extracellular tissue in promoting growth of tumors (37).

Conclusion

A novel optical molecular imaging approach was developed in this study based on simultaneous imaging of changes in glucose metabolic activity and extracellular pH in clinically isolated fresh biopsy specimens. The results of this study demonstrate high specificity of both the glucose and the pH imaging probes in detecting both early and late stages of the disease. The molecular imaging measurements correlated with the pathologic diagnosis of the biopsy samples in all cases, including early stages of the disease, and were able to distinguish between cancer and normal biopsies across all patients and anatomical sites in the head and neck cavity. The results of this study indicate that changes in intracellular glucose metabolism and cancer acidosis are initiated in the early stages of the disease, and these two selected biomarkers are correlated with the progression of the disease. Overall, based on the combination of widefield whole-tissue imaging and noninvasive topical application of the contrast media, the molecular imaging approach has significant potential to aid in detection. Future research is required to evaluate the potential of this molecular imaging approach for prognostic assessment, tumor margin detection, and monitoring of therapy response in a clinical environment.

Disclosure of Potential Conflicts of Interest

No potential conflicts of interest were disclosed.

Disclaimer

The contents of this study are solely the responsibility of the authors and do not necessarily represent the official view of the National Center for Research Resources (NCRR) or NIH.

Authors' Contributions

Conception and design: Z. Luo, M.N. Loja, D.G. Farwell, N. Nitin
Development of methodology: Z. Luo, M.N. Loja, N. Nitin
Acquisition of data (provided animals, acquired and managed patients, provided facilities, etc.): Z. Luo, M.N. Loja, D.G. Farwell, Q.C. Luu, P.J. Donald, A.Q. Truong, R. Gandour-Edwards, N. Nitin
Analysis and interpretation of data (e.g., statistical analysis, biostatistics, computational analysis): Z. Luo, M.N. Loja, D.G. Farwell, N. Nitin
Writing, review, and/or revision of the manuscript: Z. Luo, M.N. Loja, D.G. Farwell, D. Amott, N. Nitin
Administrative, technical, or material support (i.e., reporting or organizing data, constructing databases): Z. Luo, M.N. Loja, D. Amott
Study supervision: Z. Luo, N. Nitin

Grant Support

This study was supported by the NCRR, NIH, through grant UL1 RR024146 (M.N. Loja and Z. Luo) and linked award TL1 RR024145.

Information on reengineering the Clinical Research Enterprise can be obtained from http://nihroadmap.nih.gov/clinicalresearch/overview-translational.asp.

The costs of publication of this article were defrayed in part by the payment of page charges. This article must therefore be hereby marked *advertisement* in accordance with 18 U.S.C. Section 1734 solely to indicate this fact.

Received April 2, 2014; revised June 20, 2014; accepted July 15, 2014; published OnlineFirst August 19, 2014.

References

1. Jemal A, Bray F, Center MM, Ferlay J, Ward E, Forman D. Global cancer statistics. CA Cancer J Clin 2011;61:69–90.
2. Neville BW, Day TA. Oral cancer and precancerous lesions. CA Cancer J Clin 2002;52:195–215.
3. Fleskens S, Slootweg P. Grading systems in head and neck dysplasia: their prognostic value, weaknesses and utility. Head Neck Oncol 2009; 1:11.
4. Glunde K, Artemov D, Penet MF, Jacobs MA, Bhujwalla ZM. Magnetic resonance spectroscopy in metabolic and molecular imaging and diagnosis of cancer. Chem Rev 2010;110:3043–59.
5. Choy G, Choyke P, Libutti SK. Current advances in molecular imaging: noninvasive in vivo bioluminescent and fluorescent optical imaging in cancer research. Mol Imaging 2003;2:303–12.
6. Gatenby RA, Gillies RJ. Why do cancers have high aerobic glycolysis? Nat Rev Cancer 2004;4:891–9.
7. Denko NC. Hypoxia, HIF1 and glucose metabolism in the solid tumour. Nat Rev Cancer 2008;8:705–13.
8. Wike-Hooley JL, Haveman J, Reinhold HS. The relevance of tumour pH to the treatment of malignant disease. Radiother Oncol 1984;2: 343–66.
9. Dellian M, Helmlinger G, Yuan F, Jain RK. Fluorescence ratio imaging of interstitial pH in solid tumours: effect of glucose on spatial and temporal gradients. Br J Cancer 1996;74:1206–15.
10. Gatenby RA, Gawlinski ET. The glycolytic phenotype in carcinogenesis and tumor invasion: insights through mathematical models. Cancer Res 2003;63:3847–54.
11. Gatenby RA, Gillies RJ. Glycolysis in cancer: a potential target for therapy. Int J Biochem Cell Biol 2007;39:1358–66.
12. Buck AK, Herrmann K, Shen CX, Dechow T, Schwaiger M, Wester HJ. Molecular imaging of proliferation in vivo: positron emission tomography with [F-18]fluorothymidine. Methods 2009;48:205–15.
13. Jadvar H, Alavi A, Gambhir SS. 18F-FDG uptake in lung, breast, and colon cancers: molecular biology correlates and disease characterization. J Nucl Med 2009;50:1820–7.
14. Niederkohr RD, Gamie SH. F-18FDG PET as an imaging tool for detecting and staging metastatic basal-cell carcinoma. Clin Nucl Med 2007;32:491–2.
15. Plathow C, Weber WA. Tumor cell metabolism imaging. J Nucl Med 2008;49:43S–63S.

16. Visser EP, Philippens MEP, Kienhorst L, Kaanders J, Corstens FHM, de Geus-Oei LF, et al. Comparison of tumor volumes derived from glucose metabolic rate maps and SUV maps in dynamic F-18-FDG PET. J Nucl Med 2008;49:892–8.
17. Vavere AL, Biddlecombe GB, Spees WM, Garbow JR, Wijesinghe D, Andreev OA, et al. A novel technology for the imaging of acidic prostate tumors by positron emission tomography. Cancer Res 2009;69:4510–6.
18. Loja MN, Luo Z, Farwell DG, Luu QC, Donald PJ, Amott D, et al. Optical molecular imaging detects changes in extracellular pH with the development of head and neck cancer. Int J Cancer 2013;132:1613–23.
19. Rosbach KJ, Williams MD, Gillenwater AM, Richards-Kortum RR. Optical molecular imaging of multiple biomarkers of epithelial neoplasia: epidermal growth factor receptor expression and metabolic activity in oral mucosa. Transl Oncol 2012;5:160–71.
20. Bedard N, Pierce M, El-Nagger A, Anandasabapathy S, Gillenwater A, Richards-Kortum R. Emerging roles for multimodal optical imaging in early cancer detection: a global challenge. Technol Cancer Res Treat 2010;9:211–7.
21. McWilliams A, MacAulay C, Gazdar AF, Lam S. Innovative molecular and imaging approaches for the detection of lung cancer and its precursor lesions. Oncogene 2002;21:6949–59.
22. Pierce MC, Richards-Kortum R. Low-cost, portable optical imaging systems for cancer diagnosis. Conf Proc IEEE Eng Med Biol Soc 2010;2010:1093–6.
23. Pierce MC, Javier DJ, Richards-Kortum R. Optical contrast agents and imaging systems for detection and diagnosis of cancer. Int J Cancer 2008;123:1979–90.
24. Betz CS, Mehlmann M, Rick K, Stepp H, Grevers G, Baumgartner R, et al. Autofluorescence imaging and spectroscopy of normal and malignant mucosa in patients with head and neck cancer. Lasers Surg Med 1999;25:323–34.
25. Pavlova I, Williams M, El-Naggar A, Richards-Kortum R, Gillenwater A. Understanding the biological basis of autofluorescence imaging for oral cancer detection: high-resolution fluorescence microscopy in viable tissue. Clin Cancer Res 2008;14:2396–404.
26. Roblyer D, Richards-Kortum R, Sokolov K, El-Naggar AK, Williams MD, Kurachi C, et al. Multispectral optical imaging device for in vivo detection of oral neoplasia. J Biomed Opt 2008;13:024019.
27. De Veld DCG, Witjes MJH, Sterenborg HJCM, Roodenburg JLN. The status of in vivo autofluorescence spectroscopy and imaging for oral oncology. Oral Oncology 2005;41:117–31.
28. Nitin N, Carlson AL, Muldoon T, El-Naggar AK, Gillenwater A, Richards-Kortum R. Molecular imaging of glucose uptake in oral neoplasia following topical application of fluorescently labeled deoxy-glucose. Int J Cancer 2009;124:2634–42.
29. Nitin N, Rosbach KJ, El-Naggar A, Williams M, Gillenwater A, Richards-Kortum RR. Optical molecular imaging of epidermal growth factor receptor expression to improve detection of oral neoplasia. Neoplasia 2009;11:542–51.
30. Holpuch AS, Phelps MP, Desai KG, Chen W, Koutras GM, Han BB, et al. Evaluation of a mucoadhesive fenretinide patch for local intraoral delivery: a strategy to reintroduce fenretinide for oral cancer chemoprevention. Carcinogenesis 2012;33:1098–105.
31. Mallery SR, Stoner GD, Larsen PE, Fields HW, Rodrigo KA, Schwartz SJ, et al. Formulation and in-vitro and in-vivo evaluation of a mucoadhesive gel containing freeze dried black raspberries: implications for oral cancer chemoprevention. Pharm Res 2007; 24:728–37.
32. Cid YP, Pedrazzi V, de Sousa VP, Pierre MB. In vitro characterization of chitosan gels for buccal delivery of celecoxib: influence of a penetration enhancer. AAPS Pharm Sci Tech 2012;13:101–11.
33. Donnelly RF, McCarron PA, Tunney MM, David Woolfson A. Potential of photodynamic therapy in treatment of fungal infections of the mouth. Design and characterisation of a mucoadhesive patch containing toluidine blue O. J Photochem Photobiol B 2007;86:59–69.
34. Llabot JM, Manzo RH, Allemandi DA. Double-layered mucoadhesive tablets containing nystatin. AAPS Pharm Sci Tech 2002;3:E22.
35. Roblyer D, Kurachi C, Stepanek V, Williams MD, El-Naggar AK, Lee JJ, et al. Objective detection and delineation of oral neoplasia using autofluorescence imaging. Cancer Prev Res 2009;2:423–31.
36. Fang JS, Gillies RD, Gatenby RA. Adaptation to hypoxia and acidosis in carcinogenesis and tumor progression. Semin Cancer Biol 2008;18: 330–7.
37. Liu CG, Zhang L, Jiang Y, Chatterjee D, Croce CM, Huebner K, et al. Modulation of gene expression in precancerous rat esophagus by dietary zinc deficit and replenishment. Cancer Res 2005;65:7790–9.